Available online at www.sciencedirect.com

jmr&t Journal of Materials Research and Technology

journal homepage: www.elsevier.com/locate/jmrt

An innovative shear links as dampers compound of shear plates and round HSS sections

Ali Ghamari [a], Seong-Hoon Jeong [b], Chanachai Thongchom [c,**], Ramadhansyah Putra Jaya [d,*]

[a] Department of Civil Engineering, Ilam Branch, Islamic Azad University, Ilam, Iran
[b] Department of Architectural Eng, Inha University, Incheon, Republic of Korea
[c] Department of Civil Engineering, Faculty of Engineering, Thammasat School of Engineering, Thammasat University, Pathumthani, 12120, Thailand
[d] Faculty of Civil Engineering Technology, Universiti Malaysia Pahang, 26300, Kuantan, Pahang, Malaysia

ARTICLE INFO

Article history:
Received 13 March 2023
Accepted 5 July 2023
Available online 8 July 2023

Keywords:
Shear link
Metallic damper
Ultimate strength
Stiffness

ABSTRACT

Though concentrically braced frames pertain to high elastic stiffness and strength, their low ductility has been introduced as a no-desirable system in the high seismic risk zone. Utilizing passive energy dampers as a capable and economical idea, the shortcoming can be solved. Experimental and numerical studies on the pipe dampers confirmed their satiable performance in the case of ductility and dissipating energy capacity. But, it is suffered from low strength and stiffness. To overcome the shortcoming of these types of metallic dampers, in this paper, the strengthening of pipe damper with shear plates is proposed and investigated numerically and parametrically. Subsequently, the required equations (in good agreement with finite element results) were presented to design and predict the behavior o the damper. Results indicated that by reduction of the length to the height of the damper, the strength and stiffness are improved. Also, the ratio of the strength of the flanges to the strength of the web affects the behavior of the damper, and increasing this ratio reduces the stiffness and ultimate strength. Therefore, it is suggested that this ratio should be greater than 1.5.

1. Introduction

Concentrically Braced Frames (CBFs) as a conventional load-bearing system suffered from low ductility and dissipating energy capacity. However, this system pertains a great lateral strength and stiffness. To overcome this shortcoming of CBFs, the use of dampers is considered a suitable and economical solution. With a proper design, using a damper not only the performance of the system is improved, but also the damages are controlled and limited in the damper. The damage control design desires to reduce or control damage progress in structural components, which goal is generally ensured through the involvement of energy dissipation devices [1]. During severe earthquakes, inelastic responses of dampers are activated to dissipate the imposed seismic energy. It is expected that the majority of plastic deformation is concentrated in dampers, letting the main structure stay within

* Corresponding author.
** Corresponding author.
E-mail addresses: aghamari@alumni.iust.ac.ir (A. Ghamari), jeong@inha.ac.kr (S.-H. Jeong), Tchanach@engr.tu.ac.th (C. Thongchom), ramadhansyah@ump.edu.my (R. Putra Jaya).
https://doi.org/10.1016/j.jmrt.2023.07.042

elastic states [2,3]. Accordingly, numerous dampers have been introduced and discussed to achieve a high dissipating capacity for structures with reduced damage. Among the existing dampers, steel dampers are more economical and easier to manufacture than other dampers. In addition to the advantages, they had shown good performance in past earthquakes as well as in experimental and numerical studies. For this reason, engineers and researchers, have special popularity and acceptance.

In recent years, a modified pipe damper, as illustrated in Fig. 1, has been proposed by Guo and co-workers [4] that is installed between the chevron brace and floor beam. This type of damper was a modified type of pipe damper that was previously introduced by Maleki and Bagheri [5] which employed the bending mechanism of pipes for energy dissipation. Experimental studies revealed that the pipe damper provides great energy dissipation capacity but it suffered from relatively low stiffness and lateral strength. Subsequently, it was tried to overcome the shortcoming of the pipe damper using a dual pipe damper (DPD) design [6].

Researchers [7] used a single vertical pipe damper to enhance the seismic behavior of the system. Subsequently, Bincy and Usha [8] evaluated optimized DPD installation in the multi-story building frame. Results indicated that the DPD had a low stiffness of the DPD. To overcome the low stiffness of the DPD, utilizing multi-pipe dampers was proposed by Behzadfar and co-workers [9]. They concluded that the shear strength of the pipe damper has a significant effect on determining the bracing behavior. Moreover, the corresponding displacement with the maximum force was increased when the damper was used. Also, the proper choice of the dimensions of the pipe dampers increased the ductility and energy absorption of the chevron brace frame. Though these different types of pipe dampers installed between the chevron brace and floor beam improve the ductility, they cause to reduce stiffness and lateral strength which is not desirable, especially for tall structures.

In line with the research for improving the behavior of pipe dampers, the using pipe as the ring, as shown in Fig. 2, was introduced by Cheraghi and Zahrai [10]. An experimental study accomplished by Zahrai and Mortezagholi [11] showed an excellent energy absorption capacity of the rings. Correspondingly, the influence of the D/t parameter and determining the elastic stiffness and strength of the ring dampers have not been evaluated by Abbasnia et al. [12] and Andalib et al. [13]. Deihim and Kafi [14] presented a parametrical study to achieve the design procedure of the damper. Correspondingly, parametric studies were carried out by Azandariani [15] to evaluate ductility and energy dissipation and provide an analytical equation to estimate the yielding capacity of the damper.

Although changing the location of the pipe damper (used as a ring as shown in Fig. 2), enhance the performance of the system, its stiffness needs to be improved. Considering the performance of the dampers shows that the shear damper pertains to high shear stiffness and shear strength as well as high dissipating energy capacity. A shear panel damper was proposed by Nakashima et al. [16]. The damper was made of main web plates surrounding two flange plates at the top and bottom. Abebe et al. [17] reported that fracture of the shear damper was started at the corners of the shear panel and flange weld. To improve the behavior of the dampers, Chen et al. [18,19] suggested stiffing the pane with stiffeners (horizontal and vertical stiffeners). Results indicated that adding the stiffeners improved the performance of the damper in the case of stiffness and maximum displacement. Ghamari et al. [20,21] proposed to use of the shear panel to improve the behavior of CBFs. Instead of adding stiffeners, Zhang et al. [22] investigated utilizing low yield point (LYP) steel for improving the dampers which sowed a good performance. Later, the equation for the design of the element outside using a shear panel made of LYP was investigated [23].

Comparing the behavior of all types of pipe damper with shear damper shows that the shear damper pertains to higher stiffness and strength than the pipe damper but the pipe damper has great ductility and dissipating energy. Subsequently, it is expected that combing the pipe and shear damper may it ended up as a successful damper in the case of stiffness, strength, and dissipating energy capacity. Therefore, in this paper, an innovative shear damper is introduced that uses both the pipe (with a round HSS section) and the shear plate that is located at the end of the diagonal member of CBF. This damper is investigated numerically and parametrically.

2. The proposed damper

2.1. *Fabrication*

As illustrated in Fig. 3, the proposed damper consists of two main elements, web plates, and round High-Strength welded Steel (HSS) sections as main boundary element elements

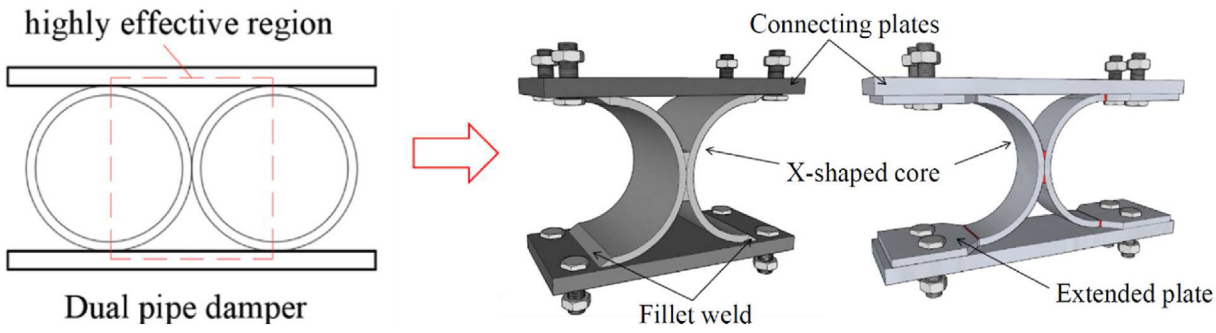

Fig. 1 – The modified pipe damper [4].

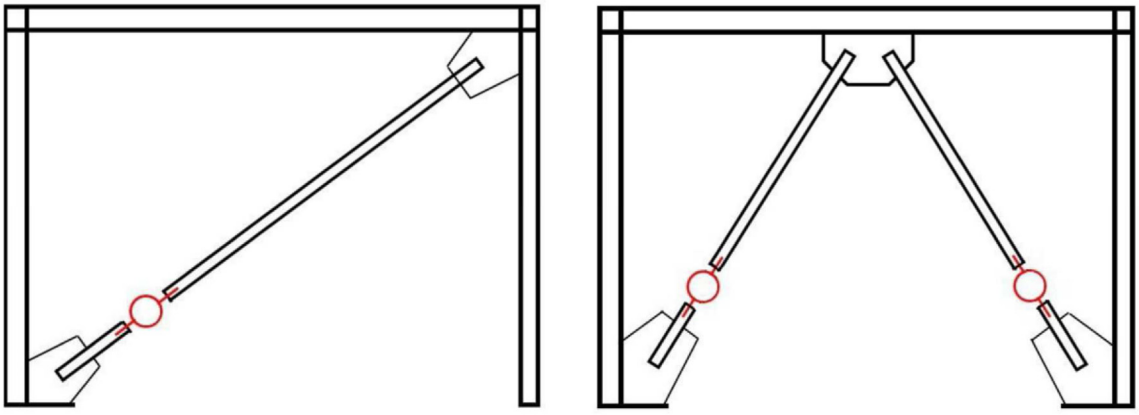

Fig. 2 – Location of steel ring damper in concentrically braced frames systems [10].

(MBE) for providing strength and stiffness. These main elements are supported by secondary elements which are the middle plate and boundary plates. It is expected that the secondary elements remain in the elastic region and do not participate in the load bearing. But they are of particular importance in the performance of the main elements. Because their nonlinear behavior will affect the performance of the damper. The middle plate and boundary plates are designed in

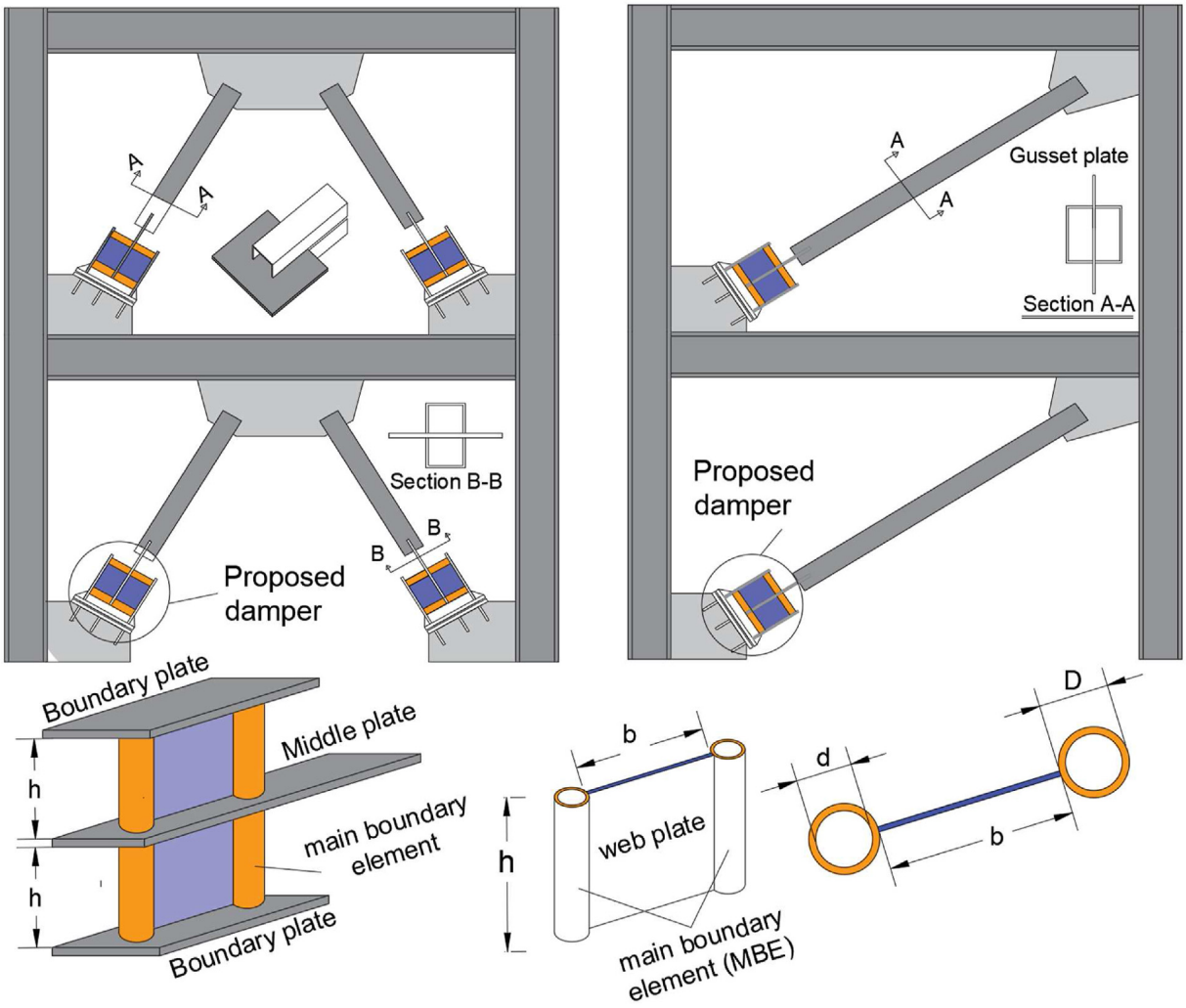

Fig. 3 – The proposed damper properties.

such a way that they remain elastic until the end of loading. Therefore, they should resist forces greater than the capacity of the main elements.

2.2. Damper mechanism

According to the AISC 341–16 [24], the parameter ρ is measured to determine the mechanism of the links. Although Eq. (1) have been presented in AISC 341–16 for I-shaped link, it can be used for other links under pure shear and bending moment. So, it is used to measure the mechanism of the proposed damper.

$$\rho = \frac{h}{M_p / V_p} \tag{1}$$

where the M_p and V_p are the plastic moment capacity and plastic shear capacity of the proposed damper. The M_p is calculated as:

$$M_p = ZF_y = \left(A_f(D+b) + A_w\frac{b}{4}\right)\left(\frac{2A_f}{A_f + A_w}\right)F_y \tag{2}$$

Where A_f and A_w are respectively the area section of round HSS and web plate. Also, the h (see Fig. 3) is the pure height of the web plate. Since the height of the MBE and web plate are the same, so, the height of the MBE is the "h".

It is expected the proposed damper act as the shear mechanism. Accordingly, Eq. (1) must be satiety. Correspondingly, to act the damper as a ductile fuse, it is expected the shear plastic hinge be formed in the web plates and two flexural plastic hinges be formed at the two ends of the MBE. Accordingly, the yielding is distributed over the web plates and two ends of the MBE.

2.3. Ultimate strength

The shear strength of the proposed damper is determined by sumation of the shear capacity of the main boundary element (made of round HSS) and the web plate element. To do so, based on the AISC 341–16 [24], Eq. (1) can be used to calculate the shear capacity of the web plate. Article F3.5b.2 of AISC 341–16 is used to determine the design shear strength, $\phi_v V_n$. For a shear link, $V_n = V_P$, where V_P is calculated as indicated in Eq. (1):

$$V_p = 0.6F_{yw}bt_w \tag{3}$$

This paper assumes that shear loading is applied not only to the web plate but also to the flange plate. Since two I-shaped sections are used for constructing the damper, a coefficient of 2 is applied:

$$V_u = 2(V_w + V_f) \tag{4}$$

For the web plate without considering the boundary HSS section, to impose shear yielding before flexural yielding, the ultimate status of the shear and bending moment capacities reached values of approximately 1.5Vp and 1.2 Mp, respectively. Further, to impose bending yielding before shear yielding of the damper's plates, the ultimate state of the shear and bending moment capacities reached values of about 0.9Vp and 1.2Mp, respectively. As $M_{pw} = \frac{tb^2}{4}F_{yw}$ and $V_p = 0.6F_{yw}bt$, the b/h ratio must be limited [21] as $\frac{b}{h} \geq 1.5$ for shear yielding, $0.9 < \frac{b}{h} < 1.5$ for shear–flexural yielding, and $\frac{b}{h} \leq 0.9$ flexural yielding. For the damper when the web plate with shear yielding and shear–flexural yielding is used, the thickness of round HSS is considered to be yielded with the web part. Accordingly, the b for this purpose is modified as $b+2t_f$.

Also, according to the AISC 341–16 [24], the nominal shear strength, *Vn*, of round HSS, according to the limit states of shear yielding and shear buckling, shall be determined as

$$V_n = 0.5F_{cr}A_g \; D/t > 100 \tag{5}$$

$$V_n = 0.5(0.6F_y)A_g \; D/t < 100, \text{low length} \tag{6}$$

where *Ag* and *D* are the gross areas and outside diameter of the round HSS, respectively. Also, the critical stress, *Fcr*, shall be the larger of

$$F_{cr} = \frac{1.60E}{\sqrt{\frac{L_v}{D}\left(\frac{D}{t}\right)^{1.25}}} \leq 0.6F_y \quad \frac{D}{t} > 100 \tag{7}$$

$$F_{cr} = \frac{0.78E}{\left(\frac{D}{t}\right)^{1.5}} \leq 0.6F_y \quad \frac{D}{t} < 100, \text{low length} \tag{8}$$

Also, L_v and t are the distance from maximum to zero shear force and the design wall thickness of the round HSS.

For the proposed damper, it is assumed that the ultimate shear strength of the round HSS section as the boundary main element is reached when two plastic hinges are formed. To do so, in this situation, the ultimate shear strength of the MBE is obtained by $\frac{4Z_f F_{yf}}{h}$. Also, if the MBE yield under shear, the shear strength of the element is reached $0.5A_g(0.6F_{yf})$. Therefore, the following equation is proposed to determine the shear capacity of the MBE.

$$V_f = max\begin{cases} \dfrac{4Z_f F_{yf}}{h} \\ 0.5A_g\left(0.6F_{yf}\right) \end{cases} \tag{9}$$

where Z_f is obtained as $Z_f = \frac{\pi(D^3 - d^3)}{6}$. Also, A_g is calculated as $A_g = \frac{\pi(D^2 - d^2)}{4}$.

2.4. Stiffness

Refs [25,26] confirmed that when a shear plate is surrounded by two flanges, the elastic stiffness of the element is following the elastic stiffness of the web plate. Also, by increasing the applied load, the stiffness of the panel, K_{damper}, is determined by the series combination of the equivalent stiffness of the web plate, K_w, and boundary element, K_f, as $K_{damper} = \frac{K_w K_f}{K_w + K_f}$. Since the web plate act as a shear element, its stiffens is obtained by:

$$K_w = n\frac{G.b.t}{h} \tag{10}$$

Where G is the shear modulus and n is the number of web plates. Since the proposed damper is made of steel, its Poison ratio is $\vartheta = 0.3$. Knowing the $G = \frac{E}{2(1+\vartheta)}$ and so the equation is

Table 1 – Properties of the models for Parametrical study.

Model	h (mm)	b/h	$\rho = \frac{h}{M_p/V_p}$	$\Phi = \frac{V_p}{V_f}$	$\frac{h}{t_w}$	t_f (mm)	d (mm)	$\frac{D}{t_f}$
1.43–0.39–1.58	140	1.43	0.39	1.58	23	5	41	10.2
1.43–0.35–0.83	140	1.43	0.35	0.83	23	10	31	5.1
1.43–0.33–0.59	140	1.43	0.33	0.59	23	15	21	3.4
1.43–0.32–0.47	140	1.43	0.32	0.47	23	20	11	2.55
0.95–0.58–1.61	210	0.95	0.58	1.61	35	5	41	10.2
0.95–0.51–0.89	210	0.95	0.51	0.89	35	10	31	5.1
0.95–0.47–0.66	210	0.95	0.47	0.66	35	15	21	3.4
0.95–0.44–0.55	210	0.95	0.44	0.55	35	20	11	2.55
0.71–0.72–2.14	280	0.71	0.72	2.14	47	5	41	10.2
0.71–0.62–1.19	280	0.71	0.62	1.19	47	10	31	5.1
0.71–0.55–0.88	280	0.71	0.55	0.88	47	15	21	3.4
0.71–0.51–073	280	0.71	0.51	0.73	47	20	11	2.55
0.57–0.87–2.68	350	0.57	0.87	2.68	58	5	41	10.2
0.57–0.73–1.48	350	0.57	0.73	1.48	58	10	31	5.1
0.57–0.64–1.10	350	0.57	0.64	1.1	58	15	21	3.4
0.57–0.59–0.92	350	0.57	0.59	0.92	58	20	11	2.55

simplified as $K_w = \frac{Ebt}{2.6h}$ where E is the modulus of elasticity. Also, the MBE act as a moment frame that stiffness is obtained by:

$$K_f = n\frac{3\pi}{16}\frac{E\left(D^4 - d^4\right)}{h^3} \tag{11}$$

2.5. *Design of elements outside the damper*

To assure the damper act as a ductile fuse, and prevents nonlinear beehive in the elements outside the main component of the damper, the component must be designed for forces greater than the capacity of the damper. Therefore, it is

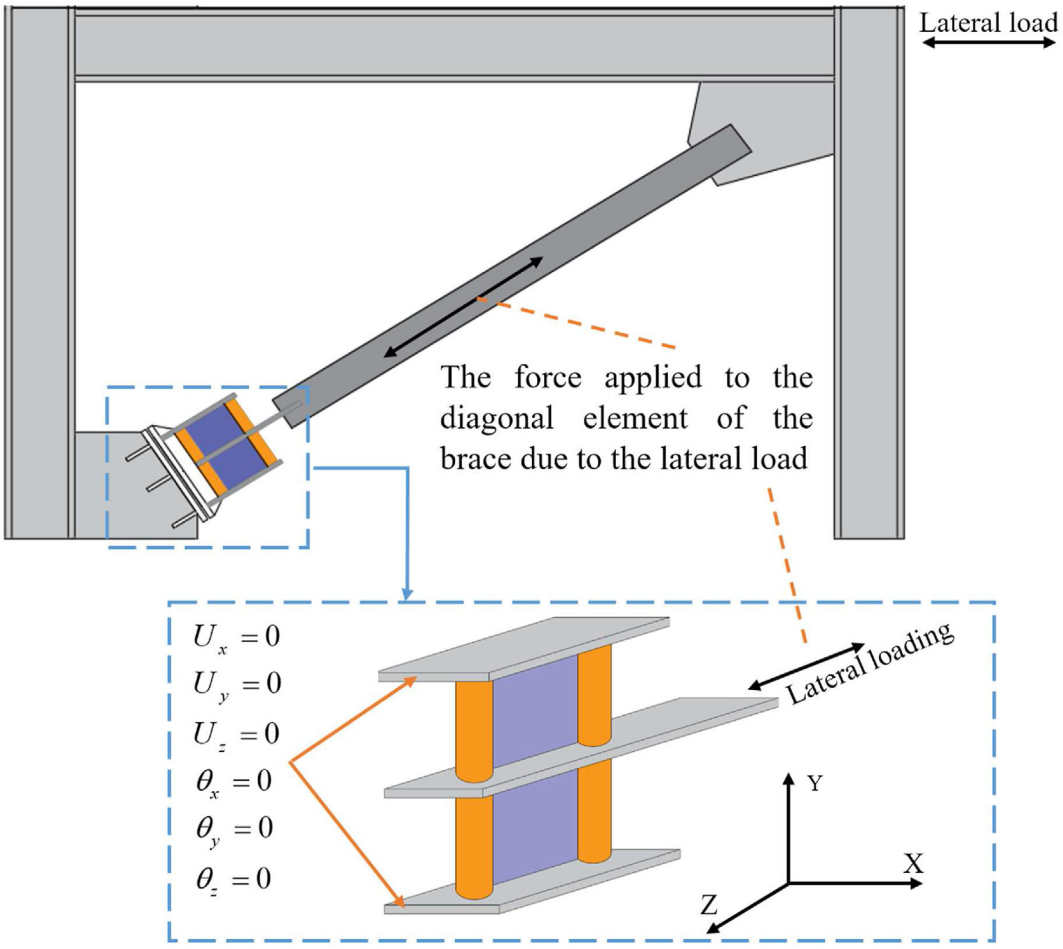

Fig. 4 – Boundary condition for the proposed damper.

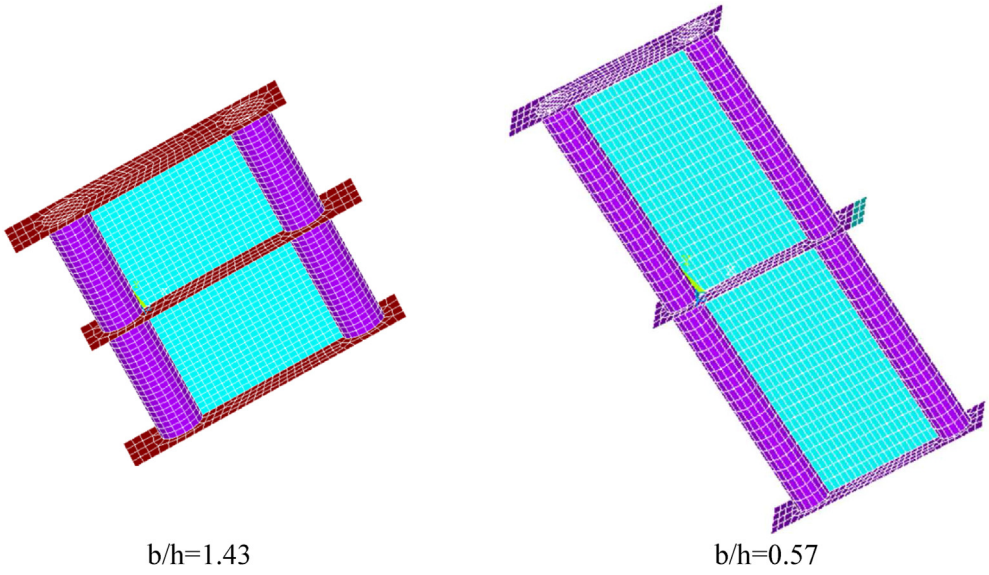

Fig. 5 – The damper modeling.

proposed to design the element to resist the maximum forces obtained by Eq. (12) and Eq. (3).

$$V_{design} = \Omega V_u \tag{12}$$

$$V_{design} = 1.25 R_y V_u = 1.5 V_u \tag{13}$$

Where the Ω and R_y is overstrength and the ratio of ultimate strength to the nominal strength of the materials, respectively. The overstrength is investigated in the next sections.

3. Parametrical study

3.1. Numerical models

A parametrical study is accomplished to investigate the behavior of the proposed damper. To do so, the effect of variables on its behavior is considered. For the parametric study on the proposed damper behavior, the FE models were designed as listed in Table 1. The name of each model indicates the values used for the parameters (b/h-ρ-Φ). The variables considered for the parametric study are the b/h ratio and the coefficients ρ and Φ. As per F3.5b of the AISC341-16, shear links should satisfy the requirements of section D1.1 [24] for highly ductile elements (considered for the models). In this standard, links with $\rho \leq 1.6$ are accounted as the shear link. Also, some researchers [21,23,27,28] categorized links with $\rho \leq 1$ as very short which was considered for the models. In this paper, although all dampers satisfy the $\rho \leq 1$, the effect of ρ on the behavior of the damper is investigated. Also, the parameter Φ is defined as the ratio of web plate strength to the MBE as $\Phi = \frac{V_p}{V_f}$. For all models, the parameters b, D, and t_w were kept constant as 200, 51, and 6 mm ($b/t_w = 33$), respectively. Also, the dampers were designed in such a way that the ratio of $\frac{D}{t_f}$ be less than 100 to satisfy the requirement of Eq. (6). This gives a fair comparison between the FE models. Also, a damper with different h and t_f is designed that gives different b/h, ρ, and Φ.

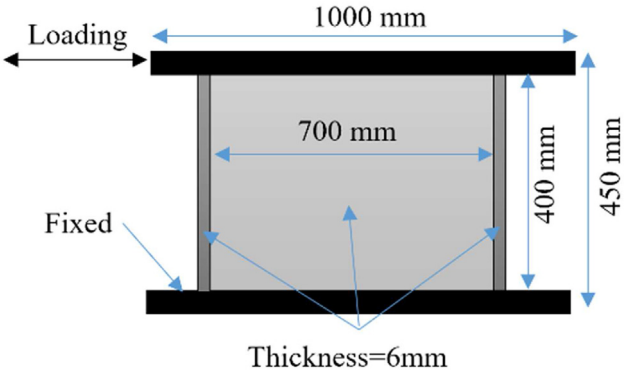

Fig. 6 – The shear panel [30].

3.2. Boundary conditions and materials

To evaluate the behavior of the proposed damper, a boundary condition is applied according to the situation where the damper is installed in the frame. To do so, the boundary conditions as illustrated in Fig. 4 are considered. All degrees of freedom were restricted at one end (location of the damper connected to the gusset plate) of the damper to create the fixed support. The loading was applied to the other end of the damper as a simplified location the diagonal element is attached to the damper. The applied loading was displacement control. To do so, it was increased until the amount of rotation reaches 8% (0.08 radians). As pointed out in article F3.4a of the AISC 341–16 [24], short/shear links attain a maximum rotation of 0.08 rad under seismic loading. Therefore, for models with a height of 140, 210, 280, and 350 mm, the displacement was determined to be 11.2, 16.8, 22.4, and 28 mm, respectively. To evaluate the hysteretic behavior of the damper, cyclic loading was applied only for the damper

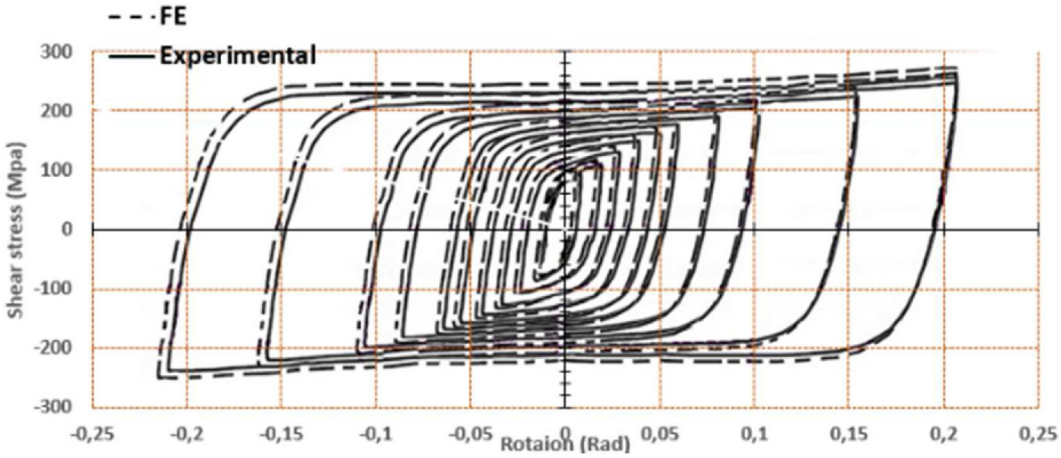

Fig. 7 – Comparison of the experimental test [30] and FE results.

with the highest and lowest confection Φ and ρ, based on the ATC24. The rationale behind the consideration of hysteretic behavior is evaluating the capability of the damper to act as a ductile fuse. Since the response of the damper is symmetric, monotonic loading was applied to reduce analysis time.

For all components of the damper, the ST37 steel with yield strength, ultimate stress, and modulus of elasticity of 240 MPa, 370 MPa, and 200 GPa was used. This data was used according to the factory catalog. The stress–strain curve of the ST37 steel is measured by the combination of elastic and plastic parts. The material model was used based on kinematic hardening. Accordingly, ANSYS incorporates the true stress–strain values, which are obtained as $\varepsilon_{true} = \ln(1+\varepsilon_{eng})$ and $\sigma_{true} = \ln(1+\sigma_{eng})$ where the subscripts "true" and "eng"

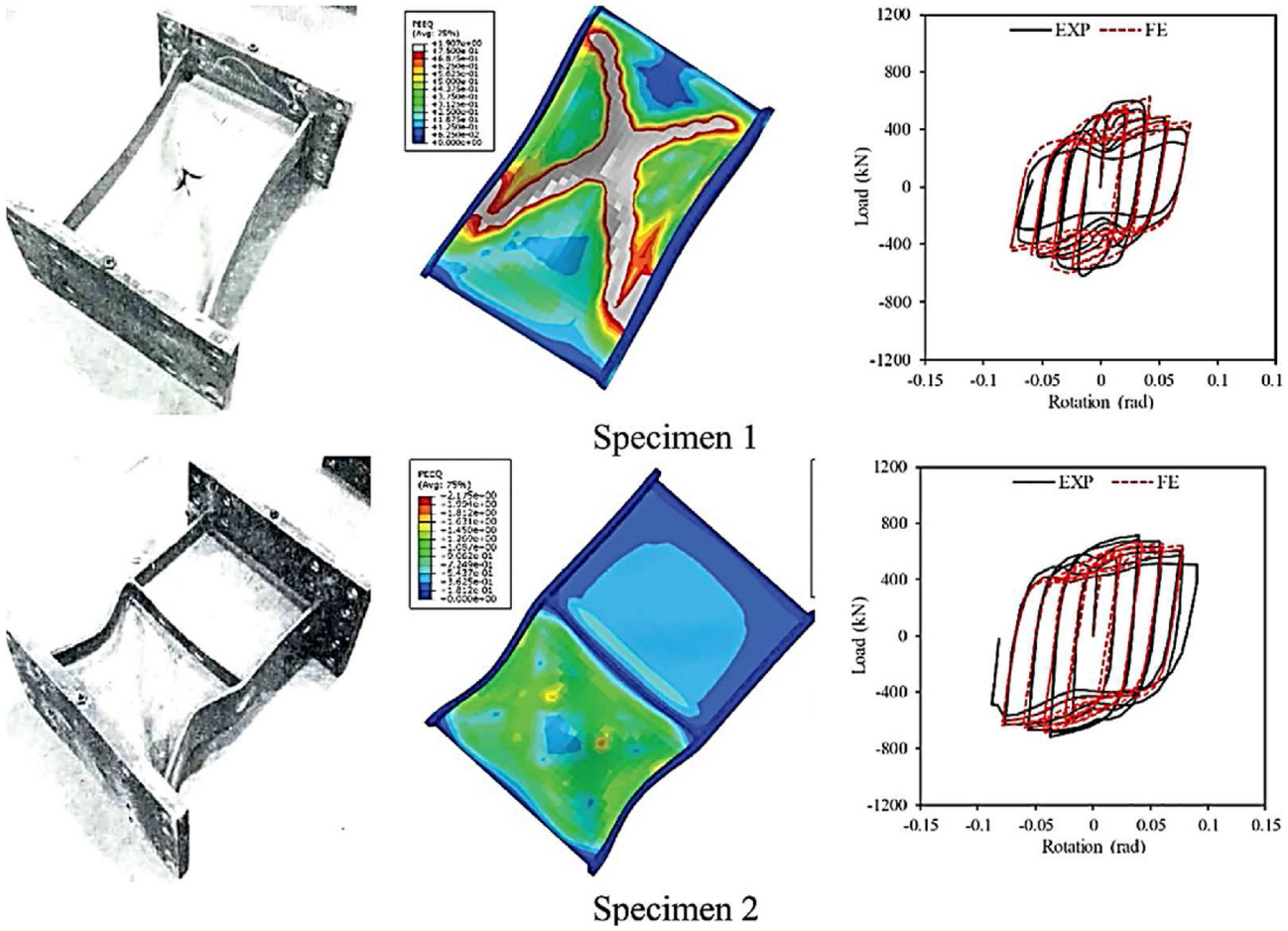

Fig. 8 – Comparison of results of the FE modeling and the experimental test [31].

refer to the true and engineering values of strain and stress [29]. Since the element of the dampers is connected together by welding, no friction is occurred between the elements. To apply the situation, the elements was meshed such an away the nods of element coincide. Then they were merged to create the fix connection.

4. Numerical study

4.1. Modeling

To simulate and analysis of the numerical model, the finite element (FE) approach was used by incorporating the ANSYS software. To do so, all damper component was simulated using SHELL 181 element. This element has a high capability to consider large displacement, nonlinearity, and buckling during analysis. The damper meshed as shown in Fig. 5. For each damper, 3614 elements were used. For each web plate and MBE, respectively, $10 \times 10 = 100$ (200 elements for two web plates) and $16 \times 10 = 160$ (640 elements for four MBEs) were used. The quality of the modeling and meshing is investigated in the verification of the FE results.

4.2. Verification of FE results

In this paper, analysis for experimental validation is performed using ANSYS software. So, In the first verification, Specimen-L2SR033 reported in Ref [27], was selected. The detail of the test model is shown in Fig. 6. Since the experimental specimen was tested under shear loading and shear deformation, it has the same mechanism (shear) and boundary conditions as the proposed damper in this paper. Subsequently, it is suitable for the verification and calibration of the FE results. In Fig. 7, the hysteresis curves of the experimental test results and FE simulation are compared that are in good agreement in linear and nonlinear regions. As the FE results were confirmed for the sample model, the other numerical models were simulated and examined to assess the behavior of the proposed damper (see Fig. 8).

In the other verification, two experimental test performed by Hjelmstad and Popov [31] were used to verify the FE results. In the experimental test, specimens with $\rho = 1.13$, were tested to investigate the effects of stiffener spacing on the performance of the shear links. These specimens were made of A36 material, with dimensions of W18-40 and a length of 711 mm. Specimen 1 had no stiffeners and Specimen 2 had one stiffener placed in the middle of the specimen. The links were shear elements with boundary stiffeners, acting as dampers, as proposed in this paper. Consequently, the boundary conditions and mechanisms employed in the experimental test were the same as those for the proposed damper. A comparison of the deformation and hysteresis curve results of the FE modeling with the results obtained in the experimental test reveals good agreement and accuracy of the FE modeling.

5. Discussion and results

5.1. Hysteresis curve

To consider the behavior of the proposed damper, its hysteresis behavior is shown in Fig. 9. For summarized, only the damper with b/h = 1.43 with t_f = 20 mm as the thickness

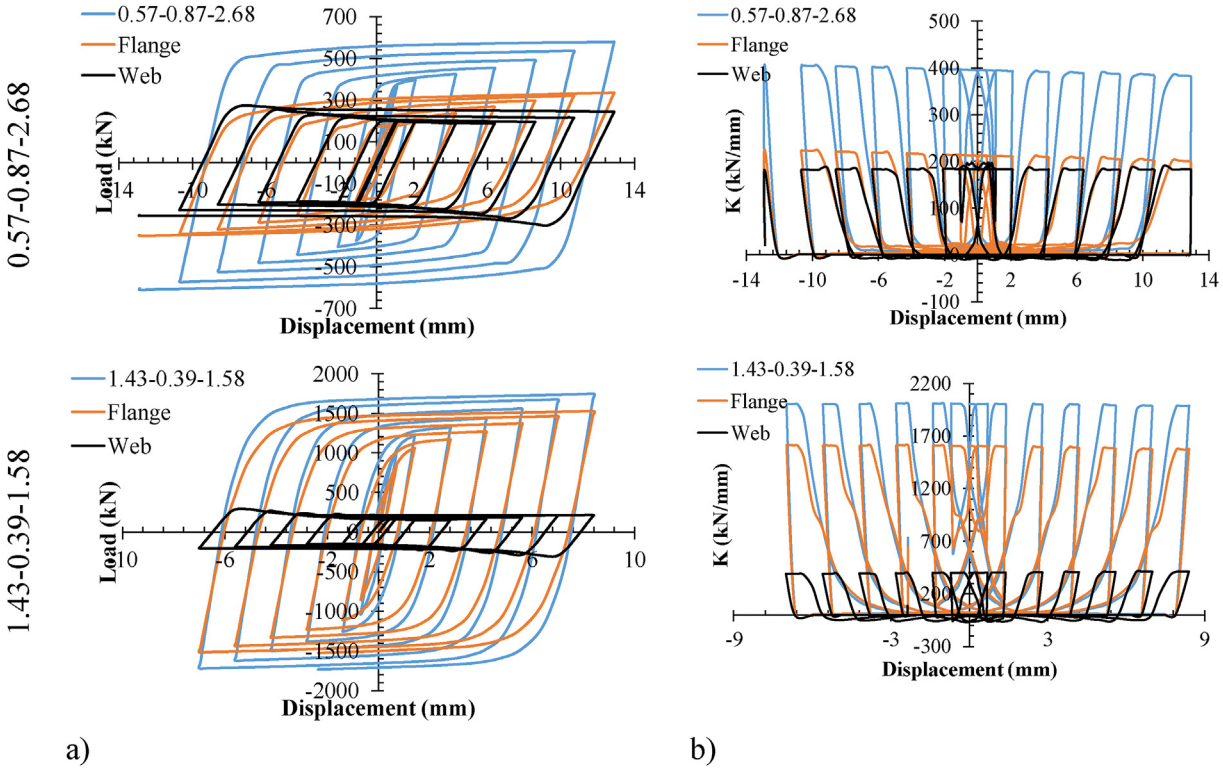

Fig. 9 – The cyclic response of the damper a) hysteresis curves b) stiffness versus displacement.

flange elements with the lowest ρ and Φ (ρ = 0.32 and Φ = 0.47) and the damper with b/h = 0.57 with t_f = 5 mm as the thickness flange elements with highest ρ and Φ (ρ = 0.87 and Φ = 2.68) are shown. results indicated that both dampers pertain to suitable hysteresis curves with stable loops and without any degradation in strength and energy dissipation. Also, stiffness versus displacement confirms that the damper behavior does not experience stiffness degradation during the applied cyclic loading. This finding confirms that the damper act as a ductile fuse to absorb the imposed energy.

Also, the yielding statues of the dampers are shown in Fig. 10. As shown in this figure, for the long damper, the yielding is started at the two ends of MBE and along with the diagonal of the web plate. By increasing the loading, the yielding is distributed over the web plate. Also, plastic hinges are formed at the two ends of the MBE. This yielding and plastic hinge formation for the damper matches the assumption that was used to drive the proposed equation. For the short link, the yielding starts at the two ends of the MBE and the web plat. For short links, the yielding is started at the mid-height of the web plate whereas for the long link, it starts along with the diagonal of the web plate. By increasing the applied load, the web plate is yielded completely, and semi-plastic hinges are formed at the two ends of the MBE. This yielding status is based on the assumption explained in Section 2.2.

5.2. *Load-rotation curves*

Since the hysteresis curve of the dampers is symmetrical, also, no degradation is seen in their hysteresis curves, and the skeleton curves of the damper are compared. In doing so, the load-rotation response of the dampers is compared in Fig. 11. As shown in this figure, with the same properties of web plate and MBE, curves of dampers with the greater b/h ratio move up that ended up with greater ultimate strength and dissipating energy. Also, by keeping the b/h ratio constant, the curve of the damper is raised by the reduction of ρ and increasing the Φ. Therefore, to achieve a damper with greater ultimate strength and dissipating energy capacity, a damper with a lower ρ, and higher b/h and Φ must be designed.

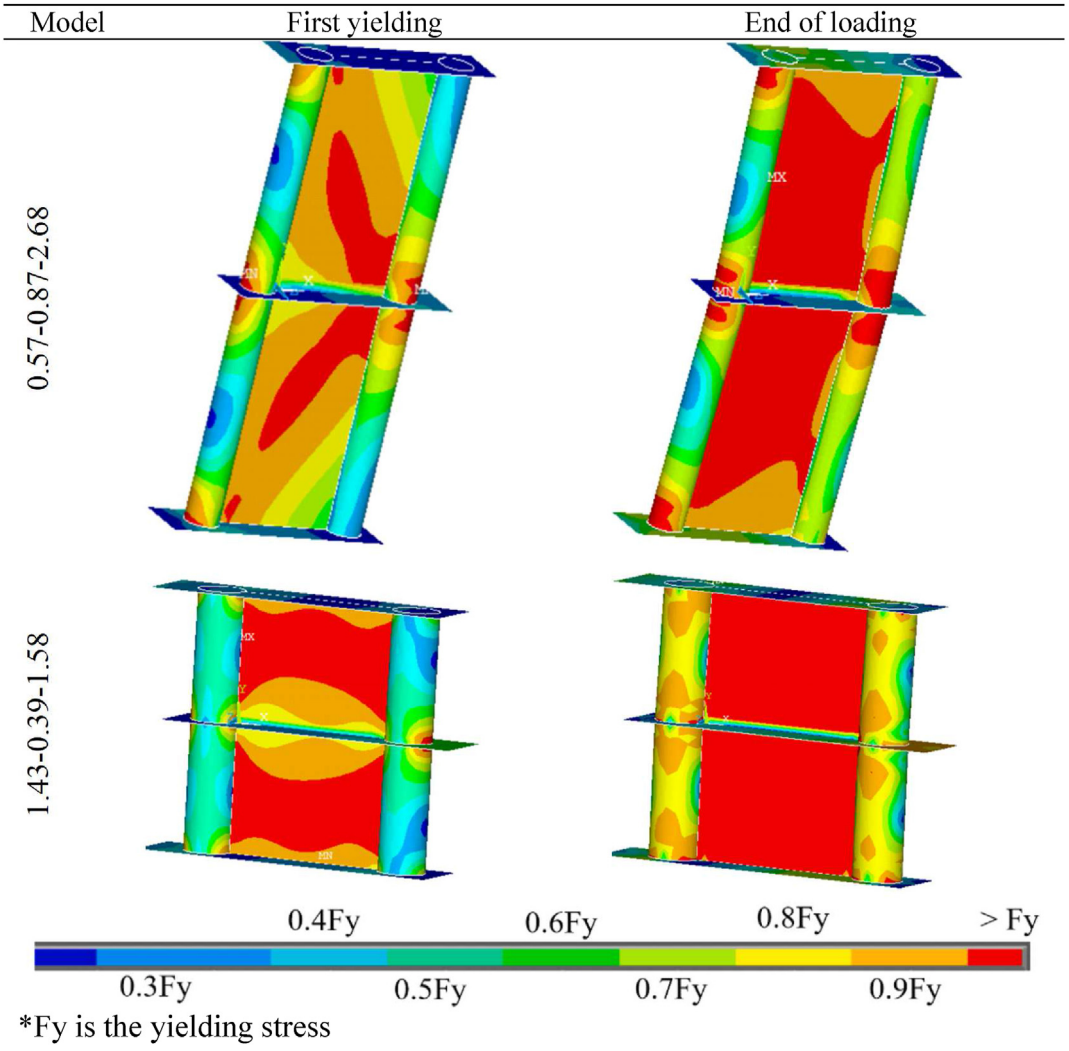

Fig. 10 – Yielding statues of the damper.

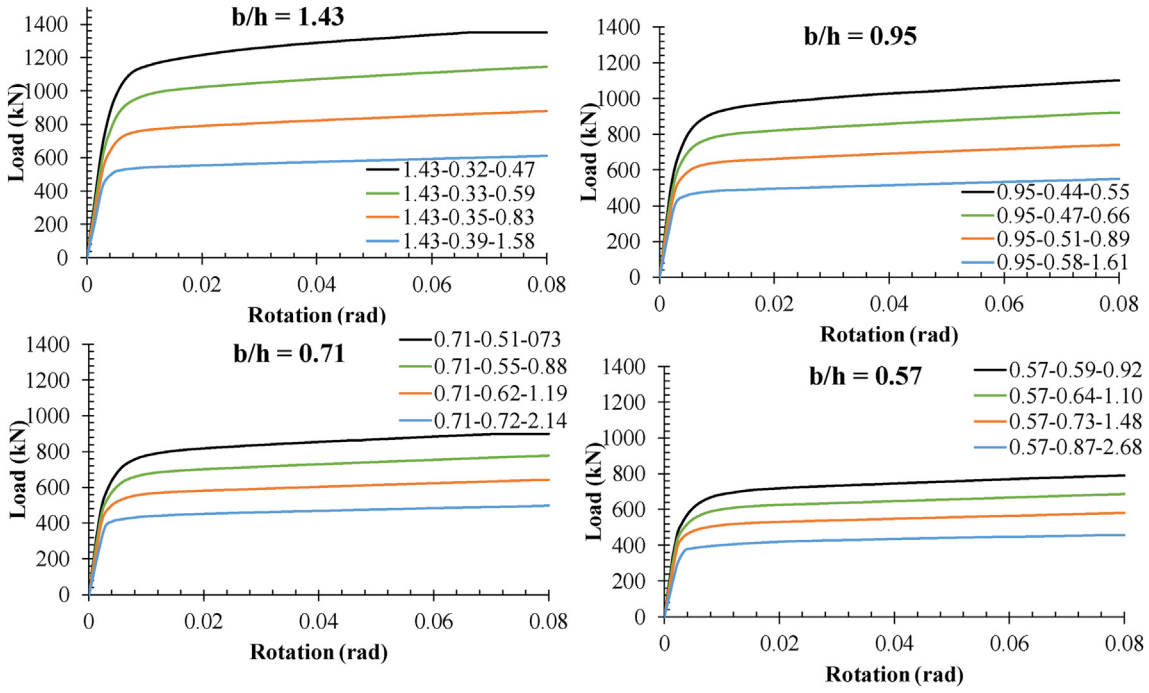

Fig. 11 – Comparing the load-rotation of the dampers.

5.3. *Considering the effect of MBE thickness on the damper behavior*

To consider the effect of the MBE's thickness on the behavior of the damper, the dampers with the same t_f and different b/h ratio are compared in Fig. 12. As shown in this figure, although by increasing the t_f the curve is improved, the improvement ratio is related to the b/h ratio. In the damper with $t_f = 5$ mm, the effect of the b/h ratio is ignorable however, in the damper with $t_f = 20$ mm, the b/h ratio plays an important role to improve the behavior of the damper. Comparing the behavior of the damper with different b/h and t_f reveal that the effect of the b/h on the response of the damper is more effective than t_f.

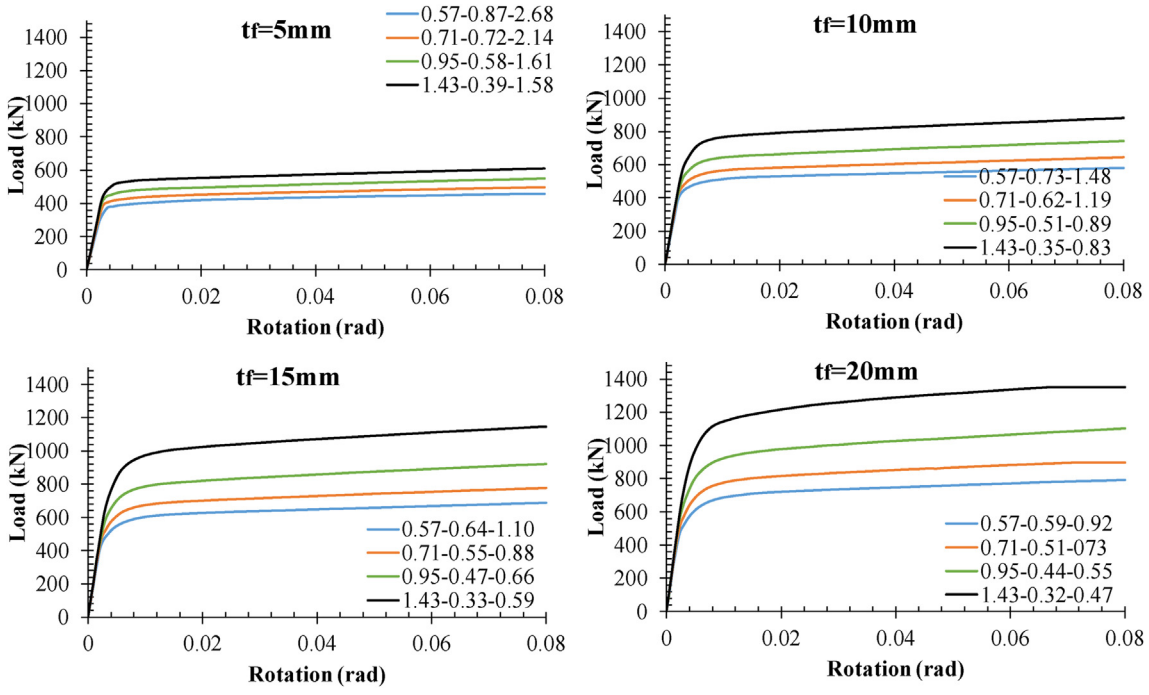

Fig. 12 – Effect of t_f on the response curve of the damper.

5.4. *Interaction of web plate and MBE*

To evaluate the behavior of the damper in the case of the interaction of the element of the dampers, the share force in the damper versus rotation is displayed in Fig. 13. To summarize, the results are plotted for dampers with $t_f = 5$ mm and $t_f = 20$ mm as dampers with thinnest and thickest flange plate in this study. This figure indicated that in the early stages of loading, the most applied load is resisted by the MBE for dampers except damper with b/h = 0.57 and $t_f = 5$ mm. At the rotation of 0.005 rad, due to the yielding of the web plate, its share has slightly reduced that causing to increase in the share of the flange plate. Also at the rotation of 0.01 rad, the share force of the web and MBE is kept constant up to the maximum rotation of the damper. According to the figure, for damper with b/h = 1.43, for $t_f = 5$ ($\Phi = 1.43$), and $t_f = 20$ mm ($\Phi = 0.47$), first, share force of the web plate reach, respectively, 34.6% and 21% whereas at the end of loading is 23% and 11%. Subsequently, in this case, the share force of the flange plate in the early stages of loading is, respectively, 65.4% and 79% whereas at the end of loading is 67% and 89%. It confirms that the share of the flange is greater than the web plate. Also, for damper with b/h = 0.57, for $t_f = 5$ ($\Phi = 0.92$), and $t_f = 20$ mm ($\Phi = 2.68$) share force of the web plate in the early stages of

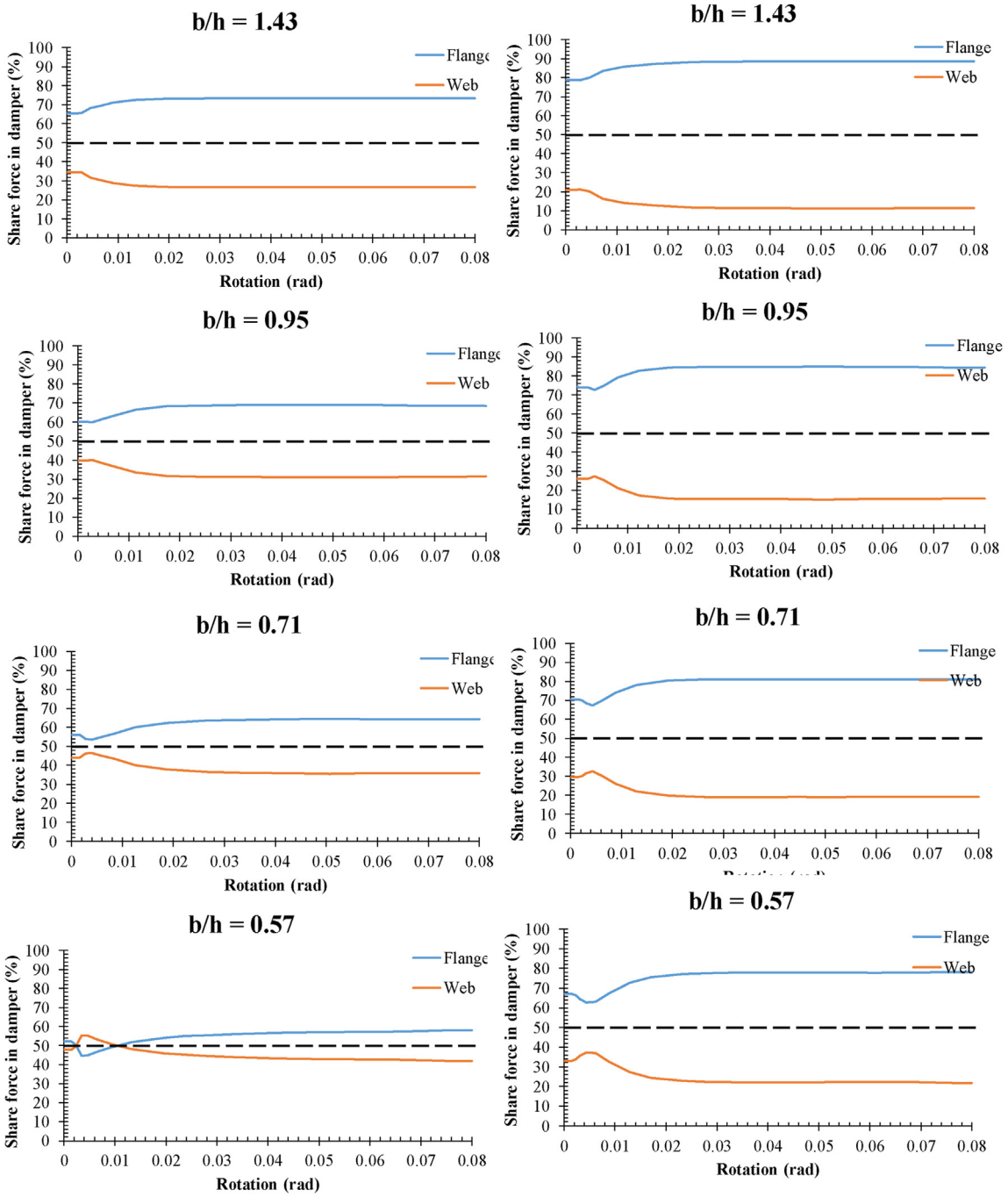

Fig. 13 – Interaction of web plate and MBD.

Table 2 – Elastic stiffness.

Model	ρ	Φ	K[a] (kN/mm)	$K_i/K_{tf\ =\ 5mm}$	$K_i/K_{b/h\ =\ 1.43}$
1.43–0.39–1.58	0.39	1.58	1141.52		
1.43–0.35–0.83	0.35	0.83	1430.49	1.25	
1.43–0.33–0.59	0.33	0.59	1658.13	1.45	
1.43–0.32–0.47	0.32	0.47	1857.38	1.63	
0.95–0.58–1.61	0.58	1.61	757.28		0.66
0.95–0.51–0.89	0.51	0.89	958.80	1.27	0.67
0.95–0.47–0.66	0.47	0.66	1105.92	1.46	0.67
0.95–0.44–0.55	0.44	0.55	1231.05	1.63	0.66
0.71–0.72–2.14	0.72	2.14	530.01		0.46
0.71–0.62–1.19	0.62	1.19	684.70	1.29	0.48
0.71–0.55–0.88	0.55	0.88	791.35	1.49	0.48
0.71–0.51–073	0.51	0.73	878.01	1.66	0.47
0.57–0.87–2.68	0.87	2.68	383.54		0.34
0.57–0.73–1.48	0.73	1.48	508.24	1.33	0.36
0.57–0.64–1.10	0.64	1.10	592.10	1.54	0.36
0.57–0.59–0.92	0.59	0.92	658.03	1.72	0.35

[a] K = Elastic stiffness.

loading are respectively 48% and 33% whereas the end of loading, they reach to 42%, 21.8%. Accordingly, except damper with b/h = 0.57 and t_f = 5 mm, the share of the flange plate in the loading is larger than the web plate.

5.5. *Stiffness*

In Table 2, the elastic stiffness, K, of the FE models is listed and compared. The elastic stiffness of the models is measured as a slope of load–displacement curves. Results indicated that by increasing the thickness of round HSS (that causes to increase in the moment of inertia) from 5 mm to 20 mm the elastic stiffness of the damper is increased between 25% and 72% which is based on the other parameters of the dampers. For dampers with b/h = 1.43 and 0.95 that represent the web plate with shear mechanism, by increasing the t_f, the improvement of elastic stiffness reaches around 25%–63% but, for damper with b/h = 0.75 and b/h = 0.57, the elastic stiffness is improved respectively by 29%–66% and 33%–72%. It is confirmed that when the b/h is lower than 0.9 (web plate with flexural mechanism), the characterization of round HSS on the elastic stiffens are more effective than damper with b/h > 0.9. in the fourth column of the table, the elastic stiffness of dampers is divided by damper with h = 140 mm. it is expected to reduce

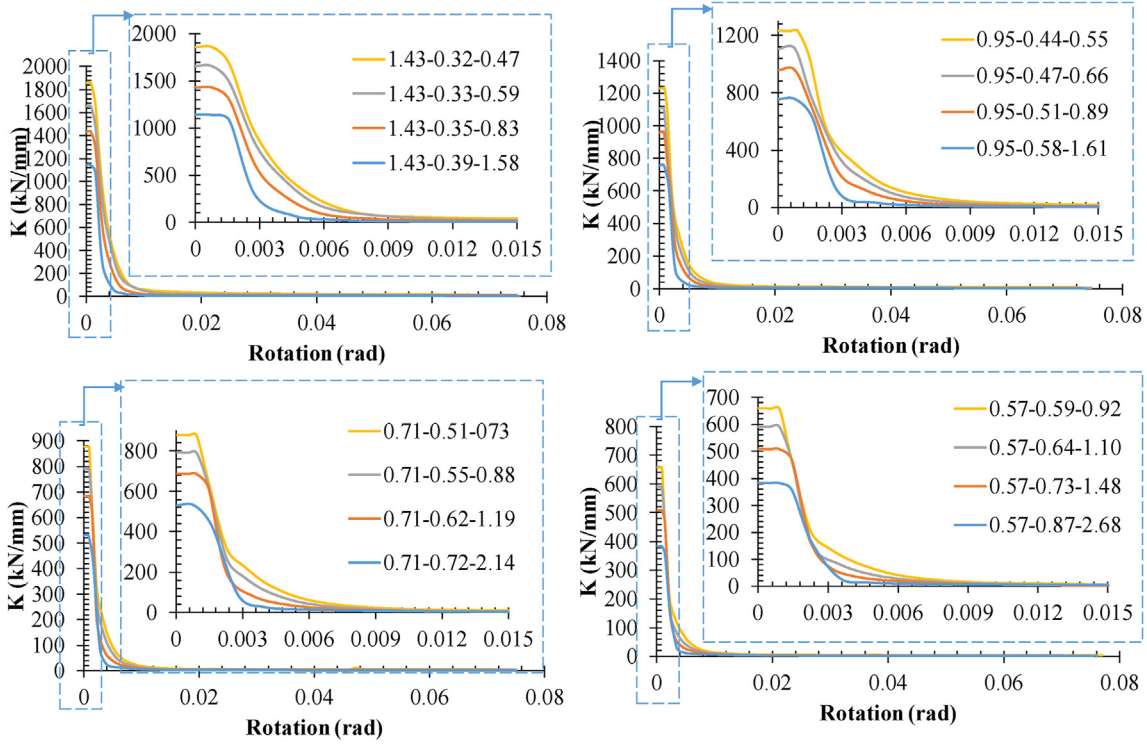

Fig. 14 – Stiffness versus rotation for dampers.

Table 3 – The ultimate strength of the damper.

Model	ρ	Φ	Fu[a] (kN)	$Fu,_i/Fu,_{tf\ =\ 5mm}$	$Fu,_i/Fu,_{b/h\ =\ 1.43}$
1.43–0.39–1.58	0.39	1.58	610.79		
1.43–0.35–0.83	0.35	0.83	879.37	1.44	
1.43–0.33–0.59	0.33	0.59	1146.57	1.88	
1.43–0.32–0.47	0.32	0.47	1349.10	2.21	
0.95–0.58–1.61	0.58	1.61	549.09		0.90
0.95–0.51–0.89	0.51	0.89	740.45	1.35	0.84
0.95–0.47–0.66	0.47	0.66	921.90	1.68	0.80
0.95–0.44–0.55	0.44	0.55	1101.43	2.01	0.82
0.71–0.72–2.14	0.72	2.14	497.78		0.81
0.71–0.62–1.19	0.62	1.19	643.55	1.29	0.73
0.71–0.55–0.88	0.55	0.88	777.26	1.56	0.68
0.71–0.51–073	0.51	0.73	883.69	1.78	0.66
0.57–0.87–2.68	0.87	2.68	457.02		0.75
0.57–0.73–1.48	0.73	1.48	580.25	1.27	0.66
0.57–0.64–1.10	0.64	1.10	687.13	1.50	0.60
0.57–0.59–0.92	0.59	0.92	791.87	1.73	0.59

[a] Fu = Ultimate strength.

Table 4 – The overstrength of the dampers.

Model	ρ	Φ	Ω	$\Omega_i/\Omega,_{tf\ =\ 5mm}$	$\Omega_i/\Omega,_{b/h\ =\ 1.43}$
1.43–0.39–1.58	0.39	1.58	2.29		
1.43–0.35–0.83	0.35	0.83	1.95	0.85	
1.43–0.33–0.59	0.33	0.59	2.08	0.91	
1.43–0.32–0.47	0.32	0.47	2.16	0.94	
0.95–0.58–1.61	0.58	1.61	1.46		1.02
0.95–0.51–0.89	0.51	0.89	1.94	1.32	1.07
0.95–0.47–0.66	0.47	0.66	2.05	1.40	1.13
0.95–0.44–0.55	0.44	0.55	2.10	1.43	1.18
0.71–0.72–2.14	0.72	2.14	1.53		1.36
0.71–0.62–1.19	0.62	1.19	1.61	1.05	1.43
0.71–0.55–0.88	0.55	0.88	1.94	1.27	1.50
0.71–0.51–073	0.51	0.73	2.01	1.31	1.58
0.57–0.87–2.68	0.87	2.68	1.14		1.70
0.57–0.73–1.48	0.73	1.48	1.55	1.36	1.78
0.57–0.64–1.10	0.64	1.10	1.72	1.51	1.88
0.57–0.59–0.92	0.59	0.92	1.93	1.70	1.97

the elastic stiffness by increasing the h which is confirmed by the results. Results indicated that increasing the height of the damper from 140 mm to 210, 280, and 350 mm caused to increase of height by 1.5, 2.0, and 2.5 times, and the elastic stiffness is reduced by around 33%, 44%, and 66%. It is concluded that the height of the damper is more effective than the properties of round HSS on the elastic stiffness.

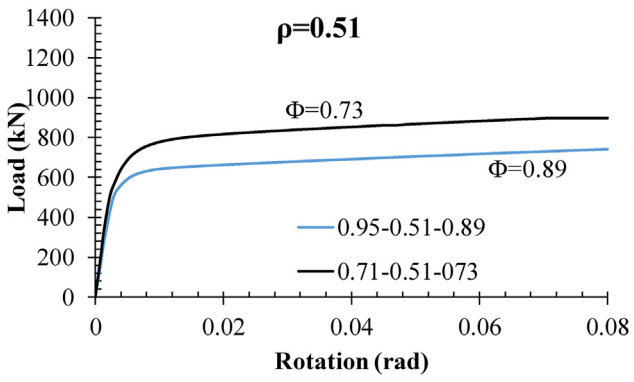

Fig. 15 – Comparing the load-rotation curve of the damper with the same ρ and different Φ

Although the elastic stiffness of the damper is affected by the web plate and round HSS, the stiffness in the nonlinear zone is not related to the mentioned elements. Referring to Fig. 14, around the rotation of 0.01 rad, the stiffness of dampers coincides. Therefore, the properties of the damper's component affect the stiffness while the rotation of the damper is less than 0.01 rad.

5.6. *Ultimate strength*

Ultimate strength as an important parameter is investigated in this section. To do so, the ultimate strength of the FE models is listed in Table 3. Referring to the results, by increasing the thickness of round HSS (that caused to increase the moment of inertia) from 5 mm to 20 mm the Fu is improved between 1.44 and 2.01 times. For dampers with b/h = 1.43 by increasing the t_f, from 5 mm to 20 mm, which is

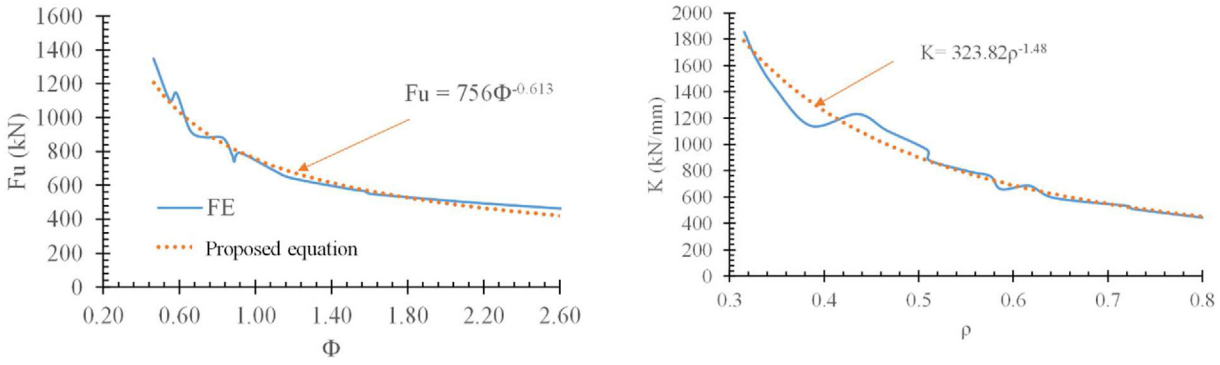

Fig. 16 – Comparing the proposed equation for primary design with FE results.

caused to changing the ρ = 0.39 to ρ = 0.32 and Φ = 1.58 to 0.47, the Fu is improved from 1.44 to 2.21. For these dampers, although changing of the ρ is not considerable, a noticeable able change in the Fu is obtained. Accordingly, other parameters such as Φ is more effective on the Fu than ρ. For dampers by increasing the t_f from 5 mm to 20 mm for the damper with b/h = 0.95 (that changes the ρ = 0.58 to 0.44 and Φ = 1.61 to 0.55), b/h = 0.71(that changes the ρ = 0.72 to 0.51 and Φ = 2.14to 0.73), and b/h = 0.51(that changes the ρ = 0.87 to 0.59 and Φ = 2.68 to 0. 92) the Fu is increased, respectively, by 2.01 times, 1.78 times, and 1.73 times. Also, by increasing the h (that reduces the ρ = 0.87 to 0.59 and Φ) from 140 mm to 210, 280, and 350 mm the Fu is reduced by 10%–18%, 19%–34%, and 25%–41%, respectively. It is concluded that the impact of t_f on the Fu of the damper is more effective than h.

5.7. *Effect of ρ and Φ on the behavior of the damper*

In previous sections, it was shown that the ρ and Φ affect the response of the damper. Accordingly, to consider the effect of ρ and Φ on the behavior of the damper, they are discussed in this section. Referring to Tables 3 and 4, results indicate that by reduction of ρ and Φ, the ultimate strength and stiffness of the damper are increased. Subsequently, to have a better consideration, in Fig. 15 the load-rotation of two dampers with the same ρ and different Φ are compared. As shown in this figure, with the same ρ, the damper with greater Φ has greater ultimate strength and dissipating energy capacity. Therefore, it is proposed to use greater Φ for the same option in the design of the damper.

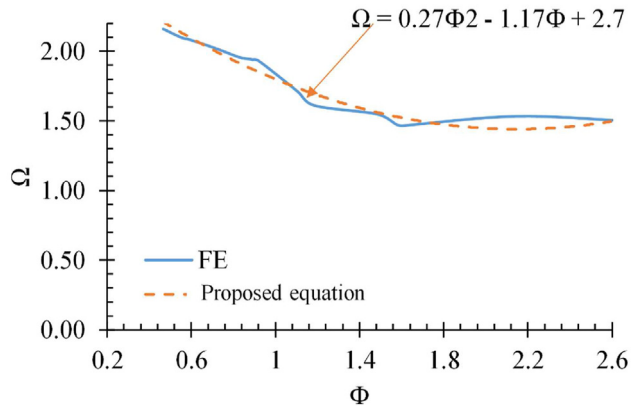

Fig. 17 – The overstrength versus the Φ

For the primary design of the damper, the following equation is proposed. These equations have been driven by the fitting of the FE results. In Fig. 16, the ultimate strength and overstrength versus Φ, and stiffness versus ρ are displayed which are in good agreement with the proposed equations.

$$F_u = 756\Phi^{-0.613} \tag{14}$$

$$K = 323.82\rho^{-1.48} \tag{15}$$

5.8. *Overstrength*

Since the element outside the proposed damper should be designed for the capacity of the damper amplified by overstrength, Ω, the Ω of the analyzed dampers are listed in Table 4. Results indicate that the ρ, Φ, t_f, and h affect the Ω. The rate of increasing the Ω due to increasing the t_f is related to the b/h ratio. Also, by reducing the b/h ratio, the Ω is enhanced from 2% to 97% which is considerable. Also, this enhancement is related to the other variable. Moreover, the reduction of the ρ cause to increase in the Ω also related to the b/h ratio and t_f. Among the parameters, the Φ has a particular effect on the Ω that is illustrated in Fig. 17. By increasing the Φ, the Ω is reduced while the Φ < 1.5. After the Φ greater than 1.5, the reduction of the Ω is ignorable. Accordingly, it is proposed to design the damper with Φ > 1.5 to have a damper with lower Ω and little sensitivity to the other variable. When the damper with lower Ω is designed, the thinner elements outside the damper are required. For primary design, Eq. (14) is proposed to predict the Ω. Also, the maximum and average amount of the Ω is, respectively, 2.29 and 1.84 which are greater than the 1.5 proposed in AISC 360–16 [31] for shear links.

$$\Omega = 0.27\Phi^2 - 1.17\Phi + 2.7 \tag{16}$$

6. Accuracy of the proposed equation

To assure the proposed results, they are compared with FE results that are listed in Table 5. Results confirm that the

Table 5 – Comparing the proposed equation results with FE results.

Model	ρ	Φ	FE		Fu-Eq	Kw	Proposed Eq/FE	
			Fu (kN)	K (kN/mm)			Fu	K
1.43–0.39–1.58	0.39	1.58	610.79	1141.52	311.17	1318.68	1.02	1.16
1.43–0.35–0.83	0.35	0.83	879.37	1430.49	433.77	1318.68	0.99	0.92
1.43–0.33–0.59	0.33	0.59	1146.57	1658.13	542.31	1318.68	0.95	0.80
1.43–0.32–0.47	0.32	0.47	1349.10	1857.38	638.51	1318.68	0.95	0.71
0.95–0.58–1.61	0.58	1.61	549.09	757.28	285.27	879.12	1.04	1.16
0.95–0.51–0.89	0.51	0.89	740.45	958.80	392.10	879.12	1.06	0.92
0.95–0.47–0.66	0.47	0.66	921.90	1105.92	493.27	879.12	1.07	0.79
0.95–0.44–0.55	0.44	0.55	1101.43	1231.05	588.79	879.12	1.07	0.71
0.71–0.72–2.14	0.72	2.14	497.78	530.01	227.62	659.34	0.91	1.24
0.71–0.62–1.19	0.62	1.19	643.55	684.70	276.80	659.34	0.86	0.96
0.71–0.55–0.88	0.55	0.88	777.26	791.35	320.32	659.34	0.82	0.83
0.71–0.51–073	0.51	0.73	883.69	878.01	358.19	659.34	0.81	0.75
0.57–0.87–2.68	0.87	2.68	421.89	383.54	227.62	527.47	1.00	1.25
0.57–0.73–1.48	0.73	1.48	580.25	508.24	276.80	527.47	0.95	1.04
0.57–0.64–1.10	0.64	1.10	687.13	592.10	320.32	527.47	0.93	0.89
0.57–0.59–0.92	0.59	0.92	791.87	658.03	358.19	527.47	0.90	0.80

proposed equation predicts the behavior of the damper in the case of elastic stiffness and ultimate strength with acceptable errors. The proposed equation for calculating the ultimate strength and elastic stiffness, predicts the parameters with a maximum error of −19% and +7%, and −29% and +25%, respectively.

7. Conclusions

In this paper, an innovative damper was introduced and its performance was investigated numerically and parametrically. Also required The findings are summarized as follows.

a) The proposed damper has excellent hysteresis curves with stable loops without any degradation and pinching. This finding confirms that the damper act as a ductile fuse to absorb the imposed energy.
b) For dampers with a small b/h ratio, the yielding is started at the two ends of MBE and also along with the diagonal of the web plate whereas by increasing the loading, it is distributed over the web plate. For the short link (long b/h), the yielding starts at the two ends of the MBE and the middle of the web plat. By increasing the applied load, the web plate is yielded completely, and semi-plastic hinges are formed at the two ends of the MBE.
c) With the same properties of web plate and MBE, curves of dampers with the greater b/h ratio move up that ended up with greater ultimate strength and dissipating energy. Also, by keeping the b/h ratio constant, the curve of the damper is raised by the reduction of ρ and increasing the Φ.
d) For damper with b/h = 1.43, for t_f = 5 (Φ = 1.43), t_f = 10 (Φ = 0.83), t_f = 15 (Φ = 0.59), and t_f = 20 mm (Φ = 0.47) share force of web plate at the begging and end of loading is respectively 34.6%–23%, 27%–18%, 23%–14%, and 21%–11%.
e) For damper with b/h = 0.57, for t_f = 5 (Φ = 0.92), t_f = 10 (Φ = 1.10), t_f = 15 (Φ = 1.48), and t_f = 20 mm (Φ = 2.68) share force of web plate at the begging and end of loading are respectively 48%–42%, 39.5%–29.7%, 35%–26.6%, and 33%–21.8%. It shows share in force for BCE is greater than the web plate even for dampers with Φ > 1.
f) Among the parameters, the Φ has a particular effect on the Ω that is illustrated in Fig. 15. By increasing the Φ, the Ω is reduced while the Φ < 1.5. After the Φ greater than 1.5, the reduction of the Ω is ignorable. Accordingly, it is proposed to design the damper with Φ > 1.5 to have a damper with lower Ω and little sensitivity to the other variable.

Declaration of Competing Interest

The authors declare that they have no known competing financial interests or personal relationships that could have appeared to influence the work reported in this paper.

Acknowledgements

The support provided by Islamic Azad University, Thammasat University and Universiti Malaysia Pahang in the form of a research grant vote number PDU213219 for this study is highly appreciated.

REFERENCES

[1] Chan RW, Albermani F. Experimental study of steel slit damper for passive energy dissipation. Eng Struct 2008;30(4):1058–66.
[2] Akcelyan S, Lignos DG, Hikino T, Nakashima M. Evaluation of simplified and state-of-the-art analysis procedures for steel frame buildings equipped with supplemental damping devices based on E-defense full-scale shake table tests. J Struct Eng 2016;142(6):04016024.

[3] Köken A, Koroglu MA. Experimental study on beam-to-column connections of steel frame structures with steel slit dampers. J Perform Constr Facil 2015;29(2):04014066.
[4] Guo Wei, Chen Xueyuan, Yu Yujie, Bu Dan, Li Shu, Fang Wenbin, et al. Development and seismic performance of bolted steel dampers with X-shaped pipe halves. Eng Struct 2021;239:112327. https://doi.org/10.1016/j.engstruct.2021.112327.
[5] Maleki S, Bagheri S. Pipe damper, Part I: experimental and analytical study. J Constr Steel Res 2010;66(9):1088–95. https://doi.org/10.1016/j.jcsr.2010.112327.
[6] Maleki S, Bagheri S. Dual-pipe damper. J Constructional Steel Res 2013;85:81–91. https://doi.org/10.1016/j.jcsr.2013.03.004.
[7] Utomo J, Moestopo M, Surahman A, Kusumastuti D. Applications of vertical steel pipe dampers for seismic response reduction of steel moment frames. In: MATEC web of conferences EACEF 2017, vol. 138; 2017. p. 02002. https://doi.org/10.1051/matecconf/201713802002.
[8] Bincy V, Usha S. Seismic performance evaluation of steel building frames with modified dual-pipe damper. IOP Conf. Series: Materials Science and Engineering, ICETEST 2020;114:012004. https://doi.org/10.1088/1757–899X/1114/1/012004.
[9] Behzadfar B, Maleki A, Yaghin Y. Improved seismic performance of chevron brace frames using multi-pipe yield dampers. Journal of Rehabilitation in Civil Engineering 2020. https://doi.org/10.22075/JRCE.2020.19792.1383. 8-4 137-155.
[10] Cheraghi A, Zahrai SM. Innovative multi-level control with concentric pipes along brace to reduce seismic response of steel frames. J Constr Steel Res 2016;127:120–35. https://doi.org/10.1016/J.JCSR.2016.07.024.
[11] Zahrai SM, Hosein Mortezagholi M. Cyclic performance of an elliptical-shaped damper with shear diaphragms in chevron braced steel frames. J Earthq Eng 2018;22:1209–32. https://doi.org/10.1080/13632469.2016.1277436.
[12] Abbasnia R, Vetr MGH, Ahmadi R, Kafi MA. Experimental and analytical investigation on the steel ring ductility. J. Sharif Sci. Technol. 2008;52:41–8.
[13] Andalib Z, Kafi MA, Kheyroddin A, Bazzaz M. Experimental investigation of the ductility and performance of steel rings constructed from plates. J Constr Steel Res 2014;103:77–88. https://doi.org/10.1016/j.jcsr.2014.07.016.
[14] Deihim M, Kafi MA. A parametric study into the new design of a steel energy-absorbing connection. Eng Struct 2017;145:22–33. https://doi.org/10.1016/j.engstruct.2017.04.056.
[15] Azandariani Mojtaba Gorji, Hamid Abdolmaleki, Azandariani Ali Gorji. Numerical and analytical investigation of cyclic behavior of steel ring dampers (SRDs). Thin-Walled Struct 2020;151:106751. https://doi.org/10.1016/j.tws.2020.106751.
[16] Nakashima M, Iwai S, Iwata M, Takeuchi T, Konomi S, Akazawa T, et al. Energy dissipation behaviour of shear panels made of low yield steel. Earthq Eng Struct Dynam 1994;23:1299–313. https://doi.org/10.1002/eqe.42902 31203.
[17] Abebe DY, Jeong SJ, Getahune BM, Segu DZ, Choi JH. Hysteretic characteristics of shear panel damper made of low yield point steel. Mater Res Innovat 2015;19:902–10. https://doi.org/10.1179/14328 91714 Z.00000 00001 219.
[18] Chen Z, Ge H, Usami T. Hysteretic performance of shear panel dampers. Adv Steel Struct 2005;2:1223–8.
[19] Chen Z, Ge H, Usami T. Hysteretic model of stiffened shear panel dampers. J Struct Eng 2006;132:478–83. https://doi.org/10.1061/(ASCE)0733-9445(2006)132:3(478).
[20] Ghamari A, Haeri H, Khaloo A, Zhu Z. Improving the hysteretic behavior of concentrically braced frame (CBF) by a proposed shear damper.Steel and composite structures. Int J 2019;30(4):383–92. https://doi.org/10.12989/scs.2019.30.4.383.
[21] Ghamari A, Kim C, Jeong S-H. Development of an innovative metallic damper for concentrically braced frame systems based on experimental and analytical studies. Struct Des Tall Special Build 2022;31(8):e1927. https://doi.org/10.1002/tal.1927.
[22] Zhang C, Zhang Z, Zhang Q. Static and dynamic cyclic performance of a low-yield-strength steel shear panel damper. J Constr Steel Res 2012;79:195–203. https://doi.org/10.1016/j.jcsr.2012.07.030.
[23] Ghadami A, Pourmoosavi Gh, Ghamari A. Seismic design of elements outside of the short low-yield-point steel shear links. J Constructional Steel Res 2021;178:106489. https://doi.org/10.1016/j.jcsr.2020.106489.
[24] AISC. AISC 341-16, seismic provisions for structural steel buildings. Chicago, IL, USA: American Institute of Steel Construction; 2016.
[25] Krawinkler H. Shear in beam-column joints in seismic design of steel frames. Eng J 1978;15(3).
[26] Safaei S, Shamlu M, Vakili A. Modeling methods and constitutive laws for nonlinear analysis of steel moment-resisting frames. J Constructional Steel Res 2022;199:107583.
[27] Shayanfar MA, Rezaeian AR, Zanganeh A. Seismic performance of eccentrically braced frame with vertical link using PBPD method. Struct Des Tall Special Build 2014;23:1–21. https://doi.org/10.1002/tal.1015.
[28] Kazemi MT, Erfani S. Special VM link element for modeling of shear–flexural interaction in frames. Struct Des Tall Special Build 2009;18:119–35. https://doi.org/10.1002/tal.395.
[29] ANSYS 17. ANSYS analysis user's manual. 2018.
[30] ANSI/AISC 360-16. Specification for structural steel buildings. Inst. Steel Constr., American; 2016. p. 1–612.
[31] Hjelmstad KD, Popov EP. Seismic behavior of active beam link in eccentrically braced frames, Rep. No. UCB/EERC-83/15. Berkeley: Earthquake Engineering Research Center, University of California; 1983.